Journal of
NANOSTRUCTURES
JNS NANOSTRUCTURES
JNS.kashanu.ac.ir

Synthesis and Charaterization of Magensium Oxide Mesoporous Microstructures Using Pluronic F127

A. Tadjarodi*, M. Sedghi, K. Bijanzad

Department of Chemistry, Iran University of Science and Technology, 16846-13114, Tehran, Iran

Article history:
Received 13/9/2012
Accepted 26/11/2012
Published online 1/12/2012

Keywords:
Magnesium oxide
Pluronic F127
Mesoporous

**Corresponding author:*
E-mail address:
tajarodi@iust.ac.ir
Phone: +98 (21) 77240516
Fax: +98 (21) 77491204

Abstract

Mesoporous MgO microstructures were synthesized using magnesium acetate tetrahydrate, ammonium oxalate monohydrate and Pluronic F127 via heating at 40 °C for 24 h and subsequent calcination. The mesoporous structure of magnesium oxide with the specific surface area of 47m^2/g, pore volume 0.30 cm^3/g and the average pore size 24 nm is produced. According to XRD studies, the diffraction peaks of the product pattern can be indexed to the cubic structure magnesium oxide with the lattice parameter of a = 4.22 Å and showing no impurities. The product was characterized by Fourier transform infrared spectroscopy, X-ray powder diffraction analysis, N_2 adsorption-desorption and Scanning electron microscopy.

2012 JNS All rights reserved

1. Introduction

Recently, investigations about the synthesis and properties of oxide nanomaterials have aroused the interest of many researchers in the interdisciplinary field of nanotechnlogy. The main reason is the remarkable physicochemical features of different oxide nanomaterials that give rise to their dramatically growing applications in science and industry [1]. Magnesium oxide, a wide band gap insulator, possesses unique properties that bring about its miscellaneous utilizations. For instance, introducing itself as an effective alkaline adsorbent, nanocrystalline MgO shows high capacities to adsorb the environmental pollutants such as acetone, benzaldehyde, trimethylacetaldehyde, ammonia, dimethylamine, methanol, acetaldehyde [2] and carbon dioxide [3]. It is also used as a support in the structure of Fe/MgO catalysts to oxidatively remove hydrogen sulfide from biogas [4]. Satisfactory bactericidal activity of nontoxic MgO nanoparticles against different Gram positive and Gram negative bacteria in aqueous environment even as an additive in paint has been proved [5,6]. Due to high surface area together with reactive morphologies, nanocrystalline MgO plays a siginificant role in the efficient catalysis of various organic reactions including: Baylis-

Hillman reaction, Strecker reaction, Wittig reaction, synthesis of organic carbonates and α-diazo-β-hydroxy esters, Mannich, cyanosilylation, Claisen-Schmidt [7, 8]. In addition, it can be used as the catalyst support for Au nanoparticles in low temperature CO oxidation [9]. Since a wide domain of reactive sites is a critical element in the field of catalysis and adsorption, high surface area and porosity are two important characteristics should be considered for MgO [3, 10]. Thus, this group of magnesium oxides could be prepared via different routes such as electrosynthesis [11], surfactant assisted [12], polyol [13] or thermal decomposition of cheap precursors [14]. Furthermore, it has found widespread applications in superconducting compounds [15], ceramic composites [16], pigments [17], lithium-ion batteries [18], pharmaceutical industry [19], humidity sensor [20] and rubber composites [21].

The unparalleled properties of MgO nanostructures stem from different sizes and morphologies which have a crucial relevance to different preparation methods and processing conditions. Thermal decomposition of $MgCO_3$ or $Mg(OH)_2$ or other precursors were known as the conventional procedures to produce MgO nanoparticles [22]. Today, numerous strategies have been employed to control the size and morphology of MgO nanostructures simultaneously precluding the drawbacks of earlier methods. For example, MgO nanoparticles were successfully produced by thermal decomposition of magnesium alkoxides [23], sol-gel [24], aerogel [25], ultrasonic [26], solid state chemical reaction [27], magnesium combustion [28], spray pyrolysis [29] and wet coprecipitation methods [30]. Magnesium oxide nanowires were generated through self-catalytic VLS growth [14], vapor-phase precursor-based [31], polyol-mediated thermolysis [32] and boron oxide-assisted catalytic growth techniques [33]. MgO nanocubes have been fabricated via thermal evaporation of Mg powders in a gas mixture of Ar and O_2 without using a catalyst [34]. MgO nanobelts were successfully prepared by direct evaporation of in situ prepared Mg_3N_2 precursor [35] as well as chemical vapor deposition [36]. Moreover, other morphologies such as nanosheets, thin films, nanoplates, fishbone- or fern-like nanostructures, nanotubes, nanotrees, nanopowders, nanocrystals, polyhedral shells, and cone-shaped branching nanostructures could be obtained respectively through wet chemical precipitation [37], sol-gel [38], chemical precipitation [39], Co-catalyzed growth [40], carbon-thermal evaporation of a MgO powder [41], carbon assisted synthesis [42], microwave assisted solvothermal [43], modified aerogel [44], thermal evaporation [45] and CVD processes [46].

In the current research, we report a facile refluxing route to generate a precursor from magnesium acetate tetrahydrate, ammonium oxalate monohydrate and Pluronic F127. Subsequent calcination of the above-mentioned compound produced mesoporous MgO microstructures.

2. Experimental procedure

2. 1. Materials

All reagents used in this work were of analytical grade, purchased from Merck Chemical Co. and used without further purification.

2. 2. Synthesis method

Magnesium acetate tetrahydrate was used as the metal source, ammonium oxalate monohydrate and the surfactant of Pluronic F127 were used as the capping ligand and stabilizer, respectively. A

mixture of metal acetate and the ligand with a molar ratio of 1:1 was added to a specific concentration of the surfactant solution (250 mL). The resulting solution was refluxed at 40 °C for 24h. Then, it was kept at 80 °C and after washing process, it was calcined at 850 °C for 4h in the electric furnace to generate magnesium oxide. The whole procedure of the synthesis has been shown in Scheme 1.

2. 3. Characterization

The powder X-ray diffraction (XRD) patterns of products were obtained on a JEOL diffractometer with monochromatized Cu Kα radiation (l = 1.5418 Å). Fourier transform infrared (FT-IR) spectra were recorded on a Shimadzu-8400S spectrometer in the range of 400–4000 cm^{-1} using KBr pellets. Scanning electron microscopy (SEM) images were taken on a Philips XL-30 with gold coating. The surface area and porosity of the as made MgO were determined by ASAP™ micromeritics 2020 adsorption analyzer.

3. Results and discussion

3. 1. XRD pattern

Chemical compositions of generated nanoparticles are verified by powder X-ray diffaraction analysis. The XRD pattern of MgO is given in Fig. 1. The diffraction peaks can be indexed to the cubic structure magnesium oxide with the lattice parameter a = 4.22 Å, which is in good agreement with the standard values (JCPDS card no. 74-1225). The diffraction peaks at 2θ values of 36.86˚, 42.82˚, 62.17˚ and 78.44˚ matching with the 111, 200, 220 and 222 of cubic MgO, respectively. There are no other peaks related to the impurities.

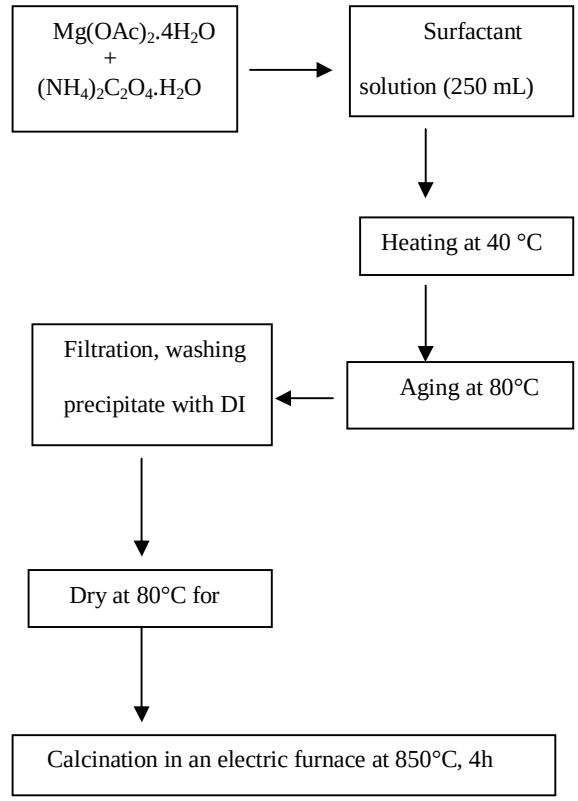

Scheme 1. Synthesis process for MgO nanostructure

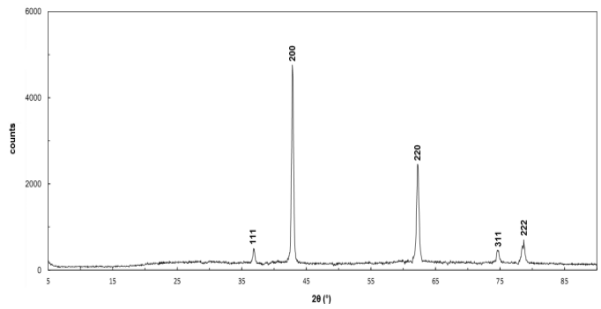

Fig. 1. XRD pattern of MgO

3. 2. SEM studies

The morphological studies of the synthesized magnesium oxide have been carried out by scanning electron microscopy. Fig. 2 displays the SEM image of the product. As it can be observed, the product is consisted of agglomerated nanoparticles constructing microstructures in the

range of 1-2 μm. They are composed of amorphous pores with the mean diameter of 26 nm.

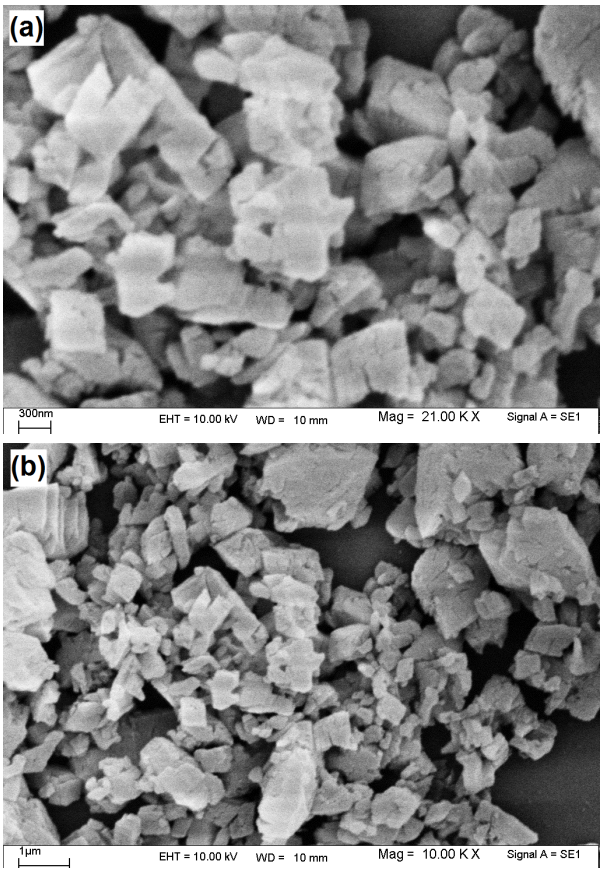

Fig. 2. SEM images of MgO (a) High magnification and (b) Low magnification

3. 3. FT-IR spectra

Fig. 3 shows the FT-IR spectra before (Fig.3-a) and after heating treatment at 850 °C for 4h (Fig. 3-b). The appeared peaks in Fig. 3-a are related to the organic section of the precursor. The absorption band at 3394 cm^{-1} is assigned to the OH stretching vibration of H_2O molecules. The observed peaks in 1641-1666 cm^{-1} are attributed to the stretching vibration of C=O, shifting to these wavenumbers from 1700 cm^{-1} as a result of metal coordination. The observed bands at 1325 and 1371cm^{-1} are due to δ(C=O) and ν_s(C-O) [47].

The appeared peak at 501 cm^{-1} belongs to Mg-O vibrations in precursor. Heating process gives rise to the removal of the organic section in MgO, as depicted vividly in Fig. 3-b. There is a strong peak at 441 cm^{-1}, which is attributed to Mg-O vibrations [23]. Calcination of the precursor at high temperatures evolves water, carbon dioxide and nitrogen oxide. Hence, MgO synthesis is confirmed by FT-IR studies.

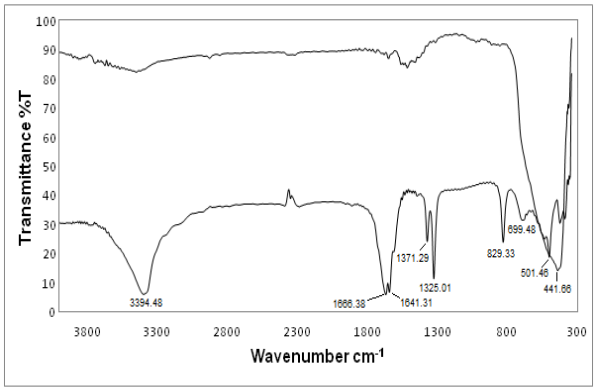

Fig. 3. FT-IR spectra of (a) precursor and (b) MgO nanostructure

3. 4. BET mesearment

Results of the BET measurements of the product show that it has mesoporous structure with irregular pores. This can be well proved by the nitrogen adsorption-desorption isotherm (Figs. 4, 5) of the product. It shows H3 hysteresis with irregular and lamellar structures that is in good agreement with SEM image. The irregularity in size and morphology of the pores is clearly seen in BJH diagrams (Fig. 5). The size distribution of the pores is in the range of 1-100 nm and the mean pore diameter is 24 nm. The parameters calculated from BET measurements are summarized in Table 1.

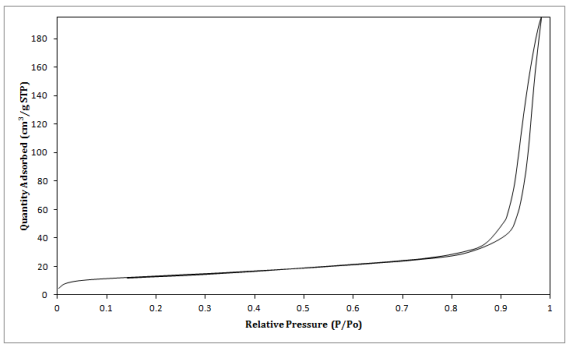

Fig. 4. Nitrogen physisorption isotherm of MgO

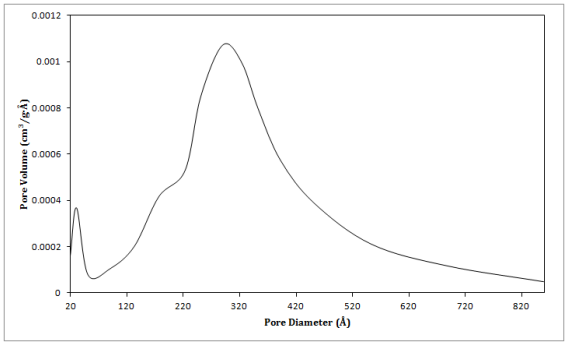

Fig. 5. Pore size distribution of MgO

Table 1. BET measurement results

Mean pore diameter (nm)	Total pore volume ($cm^3\ g^{-1}$)	$a_{s,BET}$ ($m^2\ g^{-1}$)
24	0.30	47

4. Conclusion

In summary, MgO microstructures were synthesized easily via a low temperature refluxing and following calcination at 850 °C for 4h. Magnesium acetate tetrahydrate was used as the metal source, ammonium oxalate monohydrate and the surfactant of Pluronic F127 were used as the capping ligand and stabilizer, respectively. The use of ammonium oxalate and Pluronic F 127 might be the main cause of mesoporous structures with the specific surface area of 47 m^2/g but it should be taken into consideration that other parameters such as solvent and calcination temperature might also have a noteworthy effect on the result. Upon addition of ammonium oxalate monohydrate to the solution of the surfactant and magnesium acetate tetrahydrate leads to form magnesium oxalate. The reaction was completed through heating at 40 °C for 24 h. Nucleation process on the surface of the product increased as a result of aging at 80 °C for 100 h, which formed more pores on the surface. Spongy porous MgO nanostructures with a specific surface area of 47 m^2/g and pore diameter of 24 nm were generated via calcinations at 850 °C for 4h.

Acknowledgment

The financial support of this study, by Iran University of Science and Technology and Iranian Nanotechnology Initiative, is gratefully acknowledged.

References

[1] G. R. Patzke, Y. Zhou, R. Kontic, F. Conrad, Angew. Chem. Int. Ed. 50 (2011) 826-859.

[2] A. Khaleel, P.N. Kapoor, K.J. Klabunde, Nanostruct. Mater. 11 (1999) 459-468.

[3] Z. Zhao, H. Dai, Y. Du, J. Deng, L. Zhang, F. Shi, Mater. Chem. Phys. 128 (2011) 348-356.

[4] N. Rakmak, W. Wiyaratn, C. Bunyakan, J. Chungsiriporn, Chem. Eng. J. 162 (2010) 84-90.

[5] L. Huang, D.Q. Li, Y.J. Lin, M. Wei, D.G. Evans, X. Duan, J. Inorg. Biochem. 99 (2005) 986-993.

[6] S. Makhluf, R. Dror, Y. Nitzan, Y. Abramovich, R. Jelinek, A. Gedanken, Adv. Funct. Mater. 15 (2005) 1708-1715.

[7] V. Chintareddy, M. Lakshmi Kantam, Catal. Surv. **Asia**. 15 (2011) 89-110.

[8] K. Zhu, J. Hu, C. Kübel, R. Richards, Angew. Chem. Int. Ed. 45 (2006) 7277-7281.

[9] C.J. Jia, Y. Liu, H. Bongard, F. Schuuth, J. Am. Chem. Soc. 132 (2010) 1520-1522.

[10] J. Li, W.L. Dai, K. Fan, J. Phys. Chem. C, 112 (2008) 17657-17663.

[11] G. Yuan, J. Zheng, C. Lin, X. Chang, H. Jiang, Mater. Chem. Phys. 130 (2011) 387-391.

[12] M. Rezaei, M. Khajenoori, B. Nematollahi, Powder. Technol. 205 (2011) 112-116.

[13] C.Y. Hsiao, W.M. Li, K.S. Tung, C.F. Shih, W.D. Hsu, Mater. Res. Bull. 47 (2012) 3912-3915.

[14] A. Al-Ghamdi, F. Al-Hazmi, F. Alnowaiser, R. Al-Tuwirqi, A. Al-Ghamdi, O.A. Alhartomy, F. El-Tantawy, F. Yakuphanoglu, J. Electroceram. 29 (2012) 198-203.

[15] N.A. Hamid, N.F. Shamsudin, K.M. Chin, Energ. Environ., ICEE 3rd Int. Conf. (2009) 320-323.

[16] R.G. Duan, G.D. Zhan, J.D. Kuntz, B.H. Kear, A.K. Mukherjee, Mater. Sci. Eng. A, 373 (2004) 180-186.

[17] A. Kalendová, D. Veselý, Prog. Org. Coating, 64 (2009) 5-19.

[18] J. Zhai, M. Zhao, D. Wang, Y. Qiao, J. Alloy. Compd. 502 (2010) 401-406.

[19] B.M. Choudary, K.V.S. Ranganath, J. Yadav, M. Lakshmi Kantam, Tetrahedron Lett. 46 (2005) 1369-1371.

[20] S.K. Shukla, G.K. Parashar, A.P. Mishra, P. Misra, B.C. Yadav, R.K. Shukla, L.M. Bali, G.C. Dubey, Sens. Actuators. B Chem. 98 (2004) 5-11.

[21] N.M. Ahmed, D.E. El-Nashar, S.L. Abd El-Messieh, Mater. Design. 32 (2011) 170-182.

[22] V. Stengl, S. Bakardjieva, M. Marıikova, P. Bezdiccka, J. Subrt, Mater. Lett. 57 (2003) 3998-4003.

[23] H.S. Jung, J.K. Lee, J.Y. Kim, K.S. Hong, J. Colloid. Interf. Sci. 259 (2003) 127-132.

[24] H.S. Jung, J.K. Lee, J. Young Kim, K.S. Hong, J. Solid. State Chem. 175 (2003) 278-283.

[25] O.B. Koper, I. Lagadic, A. Volodin, K.J. Klabunde, Chem. Mater. 9 (1997) 2468-2480.

[26] M.A. Alavi, A. Morsali, Ultrason. Sonochem. 17 (2010) 441-446.

[27] H. Guan, P. Wang, B. Zhao, Y. Zhu, Y. Xie, Front. Chem. China, 2 (2007) 204-208.

[28] I.S. Altman, I.E. Agranovski, M. Choi, Appl. Phys. Lett. 84 (2004) 5130-5132.

[29] D.J. Seo, S. Bin Park, Y. Chan Kang, K. Leong Choy, J. Nanopart. Res. 5 (2003) 199-210.

[30] D. Chen, L. Zhu, P. Liu, H. Zhang, K. Xu, M. Chen, J. Porous. Mat. 16 (2009) 13-18.

[31] Y. Yin, G. Zhang, Y. Xia, Adv. Funct. Mater. 12 (2002) 293-298.

[32] A. Subramania, G. Vijaya Kumar, A. R. Sathiya Priya, T. Vasudevan, Nanotech. 18 (2007) 1-5.

[33] F. Al-Hazmi, F. Alnowaiser, A. A. Al-Ghamdi, A.A. Al-Ghamdi, M.M. Aly, R. M. Al-Tuwirqi, F. El-Tantawy, Superlattice. Microst. 52 (2012) 200-209.

[34] Y. Hao, G. Meng, C. Ye, X. Zhang, L. Zhang, J. Phys. Chem. B, 109 (2005) 11204-11208.

[35] R. Ma, Y. Bando, Chem. Phys. Lett. 370 (2003) 770-773.

[36] J. Zhang, L. Zhang, X. Peng, X. Wang, Appl. Phys. A: Mater. Sci. Process, 73 (2001) 773-775.

[37] J. Hu, K. Zhu, L. Chen, C. Kübel, R. Richards, J. Phys. Chem. C, 111 (2007) 12038-12044.

[38] J.Y. Kim, H.S. Jung, K.S. Hong, J. Am. Ceram. Soc. 88 (2005) 784-787.

[39] W. Wang, X. Qiao, J. Chen, H. Li, Mater. Lett. 61 (2007) 3218-3220.

[40] Y.Q. Zhu, W.K. Hsu, W.Z. Zhou, M. Terrones, H.W. Kroto, D.R.M. Walton, Chem. Phys. Lett. 347 (2001) 337-343.

[41] R. Murugan, K. Ramamoorthy, S. Sundarrajan, S. Ramakrishna, Tetrahedron, 68 (2012) 7196-7201.

[42] K.P. Kalyanikutty, F.L. Deepak, C. Edem, A. Govindaraj, C.N.R. Rao, Mater. Res. Bull. 40 (2005) 831-839.

[43] K. Rao, K. Mahesh, S. Kumar, Bull. Mater. Sci. 28 (2005) 19-24.

[44] K.J. Klabunde, J. Stark, O. Koper, C. Mohs, D.G. Park, S. Decker, Y. Jiang, I. Lagadic, D Zhang, , J. Phys. Chem. B, 100 (1996) 12142-12153.

[45] Q. Yang, J. Sha, L. Wang, J. Wang, D. Yang, Mater. Sci. Eng. C, 26 (2006) 1097-1101.

[46] Z. Zhou, S. Xie, D. Wan, D. Liu, Y. Gao, X. Yan, H. Yuan, J. Wang, L. Song, L. Liu, W. Zhou, Y. Wang, H. Chen, J. Li, Solid. State Commun. 131 (2004) 485-488.

[47] K. Nakamoto, Infrared and Raman Spectra of Inorganic and Coordination Compounds B, sixth ed., John Wiley & Sons, Inc., Hoboken, New Jersey, 2009, pp. 62-67.